UNIVERSITY
OF TRENTO

DIPARTIMENTO DI INGEGNERIA E SCIENZA DELL'INFORMAZIONE

38123 Povo – Trento (Italy), Via Sommarive 14
http://www.disi.unitn.it

A PSO-DRIVEN SPLINE-BASED SHAPING APPROACH FOR ULTRA-WIDEBAND (UWB) ANTENNA SYNTHESIS

L. Lizzi, F. Viani, R. Azaro, and A. Massa

January 2011

Technical Report # DISI-11-044

A PSO-driven Spline-based Shaping Approach for Ultra-Wideband (UWB) Antenna Synthesis

Leonardo Lizzi, Federico Viani, Renzo Azaro, and Andrea Massa

Department of Information and Communication Technologies,

University of Trento, Via Sommarive 14, 38050 Trento - Italy

Tel. +39 0461 882057, Fax +39 0461 882093

E-mail: *andrea.massa@ing.unitn.it,*

{*leonardo.lizzi*, *federico.viani*, *renzo.azaro*}@*dit.unitn.it*

Web-site: *http://www.eledia.ing.unitn.it*

A PSO-driven Spline-based Shaping Approach for Ultra-Wideband (*UWB*) Antenna Synthesis

Leonardo Lizzi, Federico Viani, Renzo Azaro, and Andrea Massa

Abstract

This paper deals with the synthesis of *UWB* antennas by means of a PSO-driven spline-based shaping approach. In order to devise a reliable and effective solution, such a topic is analyzed according to different perspectives: 1) representation of the antenna shape with a simple and efficient description, 2) definition of a suitable description of the *UWB* Tx/Rx system, 3) formulation of the synthesis problem in terms of an optimization one, 4) integration of the modelling of the *UWB* system into a computationally efficient minimization procedure. As a result, an innovative synthesis technique based on the *PSO*-based iterative evolution of suitable shape descriptors is carefully detailed. To assess the effectiveness of the proposed method, a set of representative numerical simulations are performed and the results are compared with the measurements from experimental prototypes built according to the design specifications coming from the optimization procedure. To focus on the main advantages and features of the proposed approach, comparisons with the results obtained with a standard parametric approach are reported, as well.

Key words: Antenna Synthesis, Ultra-Wide-Band, Spline Representation, Particle Swarm Optimizer.

1 Introduction

Ultra-wideband (*UWB*) is a term commonly used to describe a wireless technology where very short low-power time pulses, which occupy a very large frequency bandwidth, are transmitted/received. Such a communication technique allows high transmission data-rates, multipath immunity, low probability of intercept, and low power consumption. Moreover, it enables the possibility for a single system to simultaneously operate in different ways (e.g., as a communication device, a locator or a radar) [1]. Since the US Federal Communication Commission (*FCC*) revision on *UWB* transmissions in 2002 [2] and the Electronic Communications Committee (*ECC*) decision in Europe about the use of *UWB* technologies [3], the design of *UWB* systems has drawn a considerable attention becoming a key topic in the framework of wireless communications.

As far as the radiating sub-system is concerned, unlike conventional narrow-band systems where modulated sinusoidal waveforms occupy small portions of the frequency spectrum, the assumption of a uniform behavior of the antenna is no longer reliable when dealing with *UWB* frequency bandwidths and the distortion of the transmitted time-domain pulses should be taken into account and carefully prevented. Consequently, *UWB* antennas turn out to be critical components of the whole system and their electrical parameters need an accurate optimization in a wide range of frequencies to minimize/reduce the signal distortions. In order to properly address such an issue, suitable techniques are necessary since a standard synthesis process aimed at determining classical frequency-domain parameters of both the transmitting antenna and the receiving one (e.g., gain, radiation patterns, reflection coefficients, and polarization) is not enough to ensure the distortionless of the *UWB* system and the correct transmission/reception of time-domain pulses. More specifically, the design of an *UWB* antenna requires customized synthesis techniques to satisfy the *UWB* requirements [4] as well as proper analysis tools for an accurate description of the antenna behaviors in the time domain [5].

Generally speaking, two main methodologies for the antenna design can be usually recognized. The former, indicated as *parametric approach*, considers a reference shape defined by a fixed number of geometric descriptors to be optimized to satisfy the project guidelines. In such a framework, different examples of *UWB* antennas have been studied

starting from simple shapes as triangular [6], circular disc [7], annular ring [8], rectangular structure [9], diamond [10][11], and bow-tie [12]. On the other hand, the so-called *building-block approach* synthesizes the antenna geometry through a suitable combination of elementary building-blocks as shown in [13] and [14].

In this paper, by exploiting the best features of both approaches, an innovative *UWB* antenna synthesis method, whose preliminary results have been presented in [15], is carefully described and analyzed. In order to design *UWB* antennas that meet the user needs, both the simplicity in describing some geometrical characteristics (e.g., the feedline extension, the groundplane, and substrate dimensions) of the parametric approach and the flexibility of a mother structure-based method are necessary to allow a fast and effective synthesis procedure. Moreover, there is the need to integrate the synthesis technique with an analysis method aimed at evaluating not only the impedance bandwidth and radiation properties but also taking into account the effects of the propagation channel on the *UWB* system. Towards this end, both the transmitting antenna and the receiving one are considered to simulate the whole system.

The outline of the paper is as follows. Section 2 gives a description of the proposed approach focusing on the representation of the antenna shape as well as on the analysis method. As for the assessment, a set of numerical and experimental results are reported and discussed (Sect. 3). Final comments and conclusions follow in Sect. 4.

2 Mathematical Formulation

The UWB antenna synthesis problem is formulated in terms of an optimization one where a set of unknown representative descriptors are tuned through an iterative process aimed at fitting suitable requirements/constraints on the electrical behavior in the *UWB* bandwidth [2][3]. Towards this end, a spline-based [16] shape generator and a *PSO* procedure [17] are used to define the convergent succession of trial solutions. By using a set of "control points" and geometrical descriptors to code the antenna shape representation, a set of trial geometries is evaluated at each iteration and updated through the *PSO* strategy until a suitable matching between estimated and required specifications is obtained. As far as the electrical behavior of each trial shape is concerned, a *MoM*-based [18] electromagnetic

simulator, developed at the *ELEctromagnetic DIAgnostic* Laboratory (ELEDIA) of the University of Trento and implemented following the guidelines in [19] and [20], is used to simulate both the transmitting antenna and the receiving one (assumed of identical shapes) as well as the propagation channel.

For the sake of clarity, the key-points of the proposed approach are detailed in the following sub-sections.

2.1 UWB Antenna Shape Representation

The first issue, addressed in dealing with *UWB* antenna synthesis, is concerned with a suitable and flexible representation of the antenna shape. To this end, there is the need to provide an antenna geometry generator (*AGG*) able to model a wide set of planar patch structures as a function of a small number of optimization variables. Accordingly, a combination of "parametric" descriptors and spline curves [16] (assumed as "building blocks") seems to be a good solution. In particular, some antenna features are expressed in terms of the values of geometrical parameters in fixed ranges. In particular, the feedline is assumed of rectangular shape as well as both the groundplane and the substrate (Fig. 1). Those parts are fully determined by fixing their extensions (i.e., their lengths and widths). The description of the antenna geometry is completed by a spline-based representation aimed at coding complex contours by means of a limited set of control points.

By assuming a symmetry with respect to the $y-z$ plane, only one half of the physical structure of the antenna has to be modeled. Let

$$\{\varphi_l;\ l=1,...,L;\ L=4\} \tag{1}$$

be the set of parametric descriptors. More specifically, φ_1 is the substrate length, φ_2 is one half of the substrate width, φ_3 is one half of the feed-line width, and φ_4 is the length of the groundplane. Moreover, $\varphi_l^{(min)} \leq \varphi_l \leq \varphi_l^{(max)}$, $\varphi_l^{(min)}$ and $\varphi_l^{(max)}$ being fixed constants that define the range of admissible variation of the l-th descriptor. As for the remaining part of the antenna geometry, let $\Delta(t) = \{x(t), y(t)\}$ be the mathematical description of the B-spline patch perimeter as a function of the curvilinear coordinate t. Such a curve turns out to be the linear combination of M-degree polynomials $\delta_{n,M}$ as follows

$$\Delta(t) = \sum_{n=1}^{N} \sum_{m=0}^{M} \delta_{n,M}\left(P_{n-M+m,t}\right), \quad M = 3 \tag{2}$$

where $P_n = (x_n, y_n)$, $n = 1, ..., N$, denotes the n-th control point whose Cartesian coordinates are (x_n, y_n). In order to avoid the generation of unrealistic structures, the following constraints are imposed, as well: $x_1 = \varphi_3$ and $x_N = 0$.

According to such a representation, a trial antenna shape A is the result of the application of the operator AGG

$$A = AGG\left(\underline{\xi}\right)$$

where

$$\underline{\xi} = \{(x_n, y_n),\ n = 1, ..., N;\ \varphi_l; l = 1, ..., L\} = \{\xi_j,\ j = 1, ..., J;\ J = 2 \times N + L\} \tag{3}$$

codes the set of variables, to be optimized to fulfill the UWB project requirements, which unequivocally identifies the corresponding geometrical model of A.

2.2 UWB Antenna System Characterization

The second step to be faced consists in identifying a fast and reliable numerical procedure to evaluate the electric behavior of each trial shape. Because of the very large frequency band of operation of UWB systems and the transmission/reception of short time pulses, a natural approach would consider a time-domain description. However, from an experimental point-of-view, a frequency domain analysis could be preferable because of the higher achievable measurement accuracy [21].

Taking into account these considerations, a time domain representation is initially adopted to define the requirements of the transmitting-receiving antenna system. Then, these requirements are "translated" in the frequency domain using the scattering parameters representation to deal with physical quantities experimentally-detectable in a straightforward and accurate way.

In order to have a distortionless behavior, the frequency domain transfer function (i.e. the ratio between the voltages at the input and the output ports of the Tx/Rx antenna

system) should satisfy the following constraints: (a) flat amplitude response and (b) phase response with a linear dependence on the frequency or, analogously, constant group delay. Under good impedance matching conditions [22] [23], the transfer function can be approximated with the scattering coefficient s_{21}. Notwithstanding such a computation usually needs the numerical modelling of the whole transmitting/receiving antenna system with a very expensive and time-consuming computational procedure. To simplify the numerical model and to reduce the computational burden, let us consider a simple method analogous to the so-called Purcell antenna gain measurement method [24]. More specifically, the two-antenna system [Fig. 2(a)] is substituted by an antenna and a reflecting surface located just in front of the transmitting device at a distance equal to one half of the Tx/Rx distance [Fig. 2(b)]. Although such an operation cannot always be performed (since an image antenna is not generally identical to the original one even though a perfectly reflecting surface of infinite area is considered [25]), however the antenna system under test fully satisfies the method hypotheses because of the axial symmetry of the reference shape (Fig. 1). Consequently, after simple manipulations, the mutual scattering coefficient s_{21} can be expressed as follows

$$s_{21} = s_{12} = s_{11} - s_{11}^{MP} \tag{4}$$

where $s_{11} = \frac{b_1}{a_1}\Big|_{a_2=0}$ is the input reflection coefficient of the original antenna system [Fig. 2(a)], while $s_{11}^{MP} = \frac{b_1^{'}}{a_1^{'}}$ is the same quantity, but in the image configuration [Fig. 2(c)]. Moreover, under the assumptions of antennas with negligible structural scattering contributions [21], the evaluation of s_{11} can be carried out by considering a single antenna that radiates in free space [Fig. 2(d)]

$$s_{11} \backsimeq s_{11}^{0} = \frac{b_0}{a_0}. \tag{5}$$

Accordingly, it appears that

$$s_{21} = s_{11}^{0} - s_{11}^{MP}. \tag{6}$$

In such a way, the whole system can be modeled by means of a single antenna instead of both transmitting and receiving devices and the s_{21} parameter can be directly estimated

from the value of s_{11} with and without the presence of an infinite metallic plate.

2.3 PSO-Based Optimization of the UWB Antenna Shape

Once an effective method to characterize a trial shape of the UWB antenna is available, there is the need to define an evolution strategy able to guide the synthesis process to a final design that fully satisfies the project guidelines and constraints defined by the user. To this end, let us reformulate the synthesis problem as an optimization one where a suitable cost function $\Omega(A)$ is minimized according to a PSO-based strategy

$$\widehat{A} = \arg\min_{A} \{\Omega(A)\} \tag{7}$$

to determine the final shape $\widehat{A} = AGG\left(\underline{\widehat{\xi}}\right)$ of the UWB antenna.

In general, evolutionary algorithms use the concept of "fitness" to represent how well a particular solution comply with the design objective. The degree of fitness to the problem at hand of each trial solution is equal to the corresponding value of the cost function. Since the design objective is to synthesize a UWB system characterized by good impedance matching conditions and by distortionless properties, the cost function Ω is accordingly defined.

Let f_1 and f_2 be the lowest and highest frequency of the band of interest, respectively. As far as the impedance matching is concerned, the following constraint is imposed

$$|s_{11}(f)| \leq \left|s_{11}^{(d)}(f)\right| \qquad f^{(min)} \leq f \leq f^{(max)} \tag{8}$$

where the superscript "$^{(d)}$" denotes the target value of the design specification. Moreover, by assuming that (8) holds true and that $H \simeq s_{21}$, the conditions for a distortionless system can be reformulated in terms of: 1) a constraint on the magnitude of s_{21} [Condition (a) - Flat amplitude response]

$$\triangle |s_{21}| \leq \triangle^{(d)} |s_{21}| \tag{9}$$

where $\triangle |s_{21}| \triangleq \max_{f^{(min)} \leq f \leq f^{(max)}} \{|s_{21}(f)|\} - \min_{f^{(min)} \leq f \leq f^{(max)}} \{|s_{21}(f)|\}$, and 2) an-

other constraint on the group delay [Condition (b) - Constant group delay]

$$\triangle\tau \leq \triangle^{(d)}\tau \tag{10}$$

where $\triangle\tau = \max_{f^{(min)}\leq f\leq f^{(max)}}\{\tau(f)\} - \min_{f^{(min)}\leq f\leq f^{(max)}}\{\tau(f)\}$, $\tau(f) = -\frac{1}{2\pi}\frac{d}{df}\{\angle s_{21}(f)\}$. Starting from these conditions on the scattering parameters, the cost function, which maps the design specifications into a fitness index, is defined as follows

$$\Omega(A) = \int_{f^{(min)}}^{f^{(max)}} \Omega_{11}(A)\,\mathcal{H}\{\Omega_{11}(A)\}\,df + \Omega_{21}(A)\,\mathcal{H}\{\Omega_{21}(A)\} + \Omega_{GD}(A)\,\mathcal{H}\{\Omega_{GD}(A)\} \tag{11}$$

where

$$\Omega_{11}(A) = \frac{|s_{11}(f)| - \left|s_{11}^{(d)}(f)\right|}{\left|s_{11}^{(d)}(f)\right|} \tag{12}$$

$$\Omega_{21}(A) = \frac{\triangle|s_{21}| - \triangle^{(d)}|s_{21}|}{\triangle^{(d)}|s_{21}|} \tag{13}$$

$$\Omega_{GD}(A) = \frac{\triangle\tau - \triangle^{(d)}\tau}{\triangle^{(d)}\tau} \tag{14}$$

$\mathcal{H}$ being the Heaviside function

$$\mathcal{H}\{\Omega\} = \begin{cases} 1 & \Omega \geq 0 \\ 0 & \Omega < 0 \end{cases}. \tag{15}$$

As far as the *PSO*-based sampling of the solution space is concerned, each particle of the swarm of dimension R codes a candidate solution $\underline{\xi}_r$ $(r = 1, ..., R)$ of the optimization problem. At each iteration k $(k = 1, ..., K)$ of the minimization process, each particle moves closer to its own best position found so far $\underline{\varsigma}_r^{(k)} = \arg\min_{k=1,...,K}\left\{\Omega\left[AGG\left(\underline{\xi}_r^{(k)}\right)\right]\right\}$ (indicated as *personal best* position) as well as towards the position of the best particle of the swarm, $\underline{\varsigma}^{(k)} = \arg\min_{r=1,...,R}\left\{\Omega\left[AGG\left(\underline{\varsigma}_r^{(k)}\right)\right]\right\}$ (referred to as *global best* position) [17] according to the rules of evolution of the PSO [26]. Starting from a swarm of particles randomly chosen (i.e., a random choice of the control points of the initial shapes without imposing a reference shape), the process stops whether $k = K$ or $k = k_{conv}$

when $\Omega\left[AGG\left(\underline{\varsigma}^{(k)}\right)\right] \leq \eta_{conv}$, η_{conv} being a user-defined threshold. Then, $\widehat{\underline{\xi}} = \underline{\varsigma}^{(k)}$ and $\widehat{A} = AGG\left(\underline{\varsigma}^{(k)}\right)$.

3 Numerical Results

In this section, a selected set of numerical results from several experiments is reported to show the behavior of the synthesis method as well as to assess its reliability and efficiency in fitting the design requirements.

Whatever the test case or experiment, if it is not specified, the project constraints have been fixed to $\left|s_{11}^{(d)}(f)\right| = -10\,dB$, $\triangle^{(d)}|s_{21}(f)| = 6\,dB$, and $\triangle^{(d)}\tau = 1\,nsec$ to guarantee suitable performances of the synthesized UWB antenna systems. As for the stochastic optimizer, a population of $R = 7$ particles has been used and the convergence threshold has been fixed to $\eta_{conv} = 10^{-3}$ with the maximum number of iterations equal to $K = 400$. Moreover, the values of the PSO control parameters have been fixed to $C_1 = C_2 = 2.0$ and $w = 0.4$. They have been selected according to the suggestions given in the reference literature where they have been found to provide good performance. For a more detailed study of convergence characteristics in correspondence with different values of these parameters, please refer to [27].

The first test case is about the synthesis of an UWB antenna operating in the range $f^{(min)} = 6\,GHz$ - $f^{(max)} = 9\,GHz$ and compliant with the guidelines of the Electronic Communications Committee (ECC) [3]. Such an experiment is aimed at analyzing the behavior of the optimization process both in terms of convergence and evolution of the antenna shape. Starting from a randomly generated perimeter [$k = 0$ - Fig. 3(a)] characterized by $N = 4$ control points, which does not fit at all the design objectives (Fig. 4) as confirmed by the value of the cost function Ω (i.e., $\Omega\left[AGG\left(\underline{\varsigma}^{(0)}\right)\right] \cong 5$), the trial solution improves until the convergence configuration [Fig. 3(d)] is found. In order to point out the main advantages of the proposed spline-based method over a parametric optimization approach, the same problem (in terms of user requirements) has been addressed by considering the reference circular geometry shown in Fig. 5. The same PSO algorithm has been used to modify the unknown parameters $\underline{\xi} = \{(x_1, y_1)\,;\, r;\, \varphi_l,\, l = 1, ..., 4\}$. Figure 6 and Figure 7 show the evolution of the trial geometry and the corresponding scattering

values during the optimization process, respectively. As it can be noticed, although the maximum number of iterations ($k = K$) has been performed, the convergence solution does not fit the whole set of project requirements ($\triangle |s_{21}(f)| > 6\,dB$). Concerning the computational issues, the plot of the cost function in correspondence with the parametric approach is compared in Fig. 8 with that of the proposed approach. Besides the wider set of possible solutions, the spline-based technique turns out to be more efficient in sampling the solution space since a better solution in reached in just $k_{conv} = 28$ iterations.

Let us now analyze the dependence of the iterative process on the dimension of the solution space. Since the generation of the spline geometry strictly depends on the number of control points that also defines the dimension of the solution space, some simulations have been performed by varying N. As a general rule, a small number of control points would decrease the dimension of the solution space allowing a faster search, but at the cost of a reduced capacity of representing complex contours. On the contrary, a larger number of control points would allow the description of a wider set of geometries and of more complex antenna shapes, even though with a higher computational burden and the need to enlarge the dimension of the swarm to fully exploit the additional degrees of freedom. In order to better understand the behavior of the optimization in correspondence with different values of N, let us consider the following quality indexes

$$F_{11} = \frac{1}{\Delta f} \int_{f^{(min)}}^{f^{(max)}} |\widehat{s}_{11}(f)|\, df \tag{16}$$

$$F_{21} = \frac{1}{\Delta f} \int_{f^{(min)}}^{f^{(max)}} \left\{ \frac{|\widehat{s}_{21}(f)| - \overline{|s_{21}(f)|}}{|\widehat{s}_{21}(f)|} \right\} df \tag{17}$$

$$F_{GD} = \frac{1}{\Delta f} \int_{f^{(min)}}^{f^{(max)}} \left\{ \frac{|\widehat{\tau}(f)| - \overline{|\tau(f)|}}{|\widehat{\tau}(f)|} \right\} df \tag{18}$$

where the superscript "$\rightarrow$" indicates the mean value, over the frequency band $\Delta f = f^{(max)} - f^{(min)}$, of the scattering parameters at the convergence $[\widehat{s}_{ij} = s_{ij}\left(\widehat{A}\right)]$. Figure 9 shows the values of the quality indexes versus N as well as the plot of k_{conv}. As expected, the number of iterations needed to find a convergence solution increases with N since the solution space becomes larger. However, the quality indexes do not proportionally improve and the optimal trade-off between computational costs and solution efficiency

turns out to be at $N = 7$ control points. In the following, this value will be assumed as reference.

After the analysis on the optimization process and on the sensitivity of the method to the antenna shape descriptors, the second part of this section is devoted to present the results from the numerical and experimental assessment. For the experimental validation, a set of antenna prototypes has been built according to the results from the numerical simulations by means of a photo-lithographic printing circuit technology and considering an Arlon substrate ($\varepsilon_r = 3.38$) of thickness $0.78\,mm$ as dielectric support. Concerning the measurements, each prototype has been fed with a coaxial line, equipped with a *SMA* connector, connected at the input port (Fig. 1). Moreover, an Anritsu Vector Network Analyzer (37397D Lightning) has been used to collect the data in a non-controlled environment and the measurements of the parameter s_{21} have been performed by considering a distance of $d = 15\,cm$ between two identical (Tx/Rx) antenna prototypes [28]. Because of the operating frequencies of UWB systems and the dimensions of the prototypes, the antennas can be reasonably considered in the far field region of each other.

The second test case deals with the synthesis of a *UWB* antenna that operates in the frequency range $4\,GHz \leqslant f \leqslant 9\,GHz$ and complies with the *FCC* standard. The values of the antenna descriptors obtained by the *PSO*-based optimization procedure are given in Tab. I and the prototype of the antenna is shown in Fig. 10. As for the electric performances, Figure 11 shows the simulated and measured behaviors of the s_{ij} parameters and of the group delay τ. As it can be observed, the antenna fits the project requirements from $f = 4\,GHz$ up to $f = 9\,GHz$ (i.e., within the *FCC* mask [2]) and the bandwidth turns out to be of $\triangle f = 5\,GHz$ (the fractional bandwidth being equal to 76.9 % according to [2]) from simulated as well as measured data. In particular, $|\widehat{s}_{11}(f)| < -10\,dB$ [Fig. 11(a)], the widest variation of the magnitude of $\widehat{s}_{21}$ is less than $5\,dB$ (i.e., $\triangle|\widehat{s}_{21}(f)| < \triangle^{(d)}|s_{21}(f)|$) [Fig. 11$(b)$ and Tab. I], and $\triangle\widehat{\tau} = 0.5\ nsec < \triangle^{(d)}\tau$ [Fig. 11(d)]. Given the separation $d = 15\,cm$ between the antennas, the achieved values for $\widehat{s}_{21}$ are reasonable and in agreement with the values obtained from the Friis formula. As regards to the dependence of $|\widehat{s}_{21}(f)|$ on the distance between the two antenna prototypes, the increase of the separation distance turns out in a shift of the plot towards lower values. As

a consequence, the value of $\triangle |\widehat{s}_{21}(f)|$ does not present significant variations with the distance.

As far as the group delay is concerned, although in a reasonable accordance with simulations, measured data present larger fluctuations probably caused by the non-controlled environment where the experimental measurements have been carried out. Nevertheless, the flat behaviors of the magnitude of s_{21} and of the group delay, or equivalently the linear trend of the phase of s_{21} [Fig. 11(c)], assure that the synthesized antenna is suitable for UWB communications where a transmitted signal should not be distorted.

The last example is concerned with a more challenging problem where a wider frequency band is required (i.e., $\Delta f = 6\,GHz$, $f^{(min)} = 4\,GHZ$ $f^{(max)} = 10\,GHZ$) and a further constraint on the dimension of the antenna is imposed for a more easy integration in commercial products (i.e., $\varphi_1^{(max)} = 35\,mm$ and $\varphi_2^{(max)} = 15\,mm$), even though a smaller threshold on the amplitude of s_{21} is fixed ($\triangle^{(d)} |s_{21}(f)| = 10\,dB$).

The descriptive parameters and the main electrical indexes of the synthesized antenna are summarized in Tab. II. Moreover, the plots of the electrical parameters over the whole frequency range are reported in Fig. 12. As expected, the antenna performances generally degrade compared to that of the previous example due to the increased band. As a matter of fact, the designed antenna has a fractional bandwidth of 85.7%. However, the maximum variation of τ is of just about $0.15\,ns$ (simulated data) and the dimensions of the antenna are very moderate ($\widehat{\varphi}_1 = 33.3\,mm$ and $\widehat{\varphi}_2 = 12.2\,mm$). On the other hand, $\triangle |\widehat{s}_{21}(f)|$ turns out to be slightly greater than the desired value ($\triangle |\widehat{s}_{21}(f)| = 12\,dB$ vs. $\triangle^{(d)} |s_{21}(f)| = 10\,dB$) since the maximum number of iterations $K = 400$ has been reached and the convergence criterion has not been satisfied. Probably, a greater dimension of the swarm and a larger number of iterations would be enough to carefully match also such a constraint, but such a setup would require very expensive computations.

The comparison between the simulation result and the data measured from the prototype (Fig. 13) further confirm the reliability of the synthesis procedure. As a matter of fact, there is an acceptable agreement between the two plots (Fig. 12) despite some reflection contributions [Fig. 12(a)] added by the non-controlled measurement environment.

4 Conclusions

In this paper, an innovative synthesis approach based on the use of a spline-based representation for *UWB* antennas has been presented. The final shape of the antenna is determined by means of a *PSO*-based optimization procedure that exploits a suitable and computationally efficient electromagnetic representation of the whole Tx/Rx *UWB* system.

The assessment has been conducted on different test cases. Firstly, the proposed technique has been tested by considering numerical examples to show the features and the behavior of the iterative procedure. In order to point out some of the main advantages of the proposed method, the same test case has been addressed with a parametric approach, as well. Secondly, we have analyzed the dependence of the synthesis method on the descriptors of the antenna shape. Finally, the synthesis results have been verified with some comparisons with the experimental data measured from the antenna prototypes.

The A conclusion, which is derived from all the numerical and experimental results obtained, is that the proposed approach represents a very promising methodology for *UWB* antenna design because of its flexibility in dealing with different user-defined requirements (e.g., *Test Case 1* and *Test Case 2*) as well as its computational efficiency.

References

[1] L. Yang and G. B. Giannakis, "Ultra-wideband communications," *IEEE Signal Processing Mag.*, pp. 26-94, Nov. 2004.

[2] US Federal Communication Commission, First Report and Order, "Revision of part 15 of the commission's rules regarding ultra-wideband transmission systems," *FCC02-48*, Apr. 2002. http://hraunfoss.fcc.gov/edocs_public/attachmatch/FCC-02-48A1.pdf

[3] Electronic Communications Committee, Draft ECC/DEC/(06)AA, "On the harmonised conditions for devices using UWB technology in bands below 10.6 GHz," *ECC/DEC/(06)AA*, 2006.

[4] Z. N. Chen, X. H. Wu, H. F. Li, N. Yang, and M. Y. W. Chia, "Consideration for source pulses and antennas in UWB radio system," *IEEE Trans. Antennas Propag.*, vol. 52, no. 7, pp. 1739-1748, Jul. 2004.

[5] X. Qing, Z. N. Chen and M. Y. W. Chia, "Characterization of ultrawideband antennas using transfer functions," *Radio Sci.*, vol. 41, RS1002, pp. 1-10, 2006.

[6] C. C. Lin, Y. C. Kan, L. C. Kuo, and H. R. Chuang, "A planar triangular monopole antenna for UWB communication," *IEEE Microwave Wireless Compon. Lett.*, vol. 15, no. 10, pp. 624-626, Oct. 2005.

[7] J. Liang, C. C. Chiau, X. Chen and C. G. Parini, "Study of a printed circular disc monopole antenna for UWB systems," *IEEE Trans. Antennas Propag.*, vol. 53, no. 11, pp. 3500-3504, Nov. 2005.

[8] Y. Ren and K. Chang, "An annular ring antenna for UWB communications," *IEEE Antennas Wireless Propag. Lett.*, vol. 5, pp. 275-276, 2006.

[9] J. Jung, W. Choi, and J. Choi, "A small wideband microstrip-fed monopole antenna," *IEEE Microwave Wireless Compon. Lett.*, vol. 15, no. 10, pp. 703-705, Oct. 2005.

[10] G. Lu, S. von der Mark, I. Korisch, L. J. Greenstein, and P. Spasojevic, "Diamond and rounded diamond antennas for ultrawide-band communications," *IEEE Antennas Wireless Propag. Lett.*, vol. 3, pp. 249-252, 2004.

[11] X. H. Wu and Z. N. Chen, "Design and optimization of UWB antennas by a powerfull CAD tool: PULSE KIT," *Proc. IEEE Antennas Propag. Int. Symp.*, vol. 2, pp. 1756-1759, Jun. 2004.

[12] K. Kiminami, A. Hirata, and T. Shiozawa, "Double-sided printed bow-tie antenna for UWB communications," *IEEE Antennas Wireless Propag. Lett.*, vol. 3, pp. 152-153, 2004.

[13] J. M. Johnson and Y. Rahmat-Samii, "Genetic algorithms and method of moments (GA/MOM) for the design of integrated antennas," *IEEE Trans. Antennas Propag.*, vol. 47, no. 10, pp. 1606-1614, Oct. 1999.

[14] F. J. Villegas, T. Cwik, Y. Rahmat-samii, and M. Manteghi, "A parallel electromagnetic genetic-algorithm optimization (EGO) application for patch antenna design," *IEEE Trans. Antennas Propag.*, vol. 52, no. 9, pp. 2424-2435, Sep. 2004.

[15] L. Lizzi, F. Viani, R. Azaro, and A. Massa, "Optimization of a spline-shaped UWB antenna by PSO," *IEEE Antennas Wireless Propag. Lett.*, vol. 6, pp. 182-185, 2007.

[16] C. De Boor, *A Practical Guide to Spline*. Springer, New York, 2001.

[17] J. Robinson and Y. Rahmat-Samii, "Particle Swarm Optimization in Electromagnetics," *IEEE Trans. Antennas Propag.*, vol. 52, no. 2, pp. 397-407, Feb. 2004.

[18] R. F. Harrington, *Field Computation by Moment Methods*. Malabar, FL: Robert E. Krieger, 1987.

[19] C. A. Balanis, *Advanced Engineering Electromagnetics*. New York, NY: John Wiley & Sons, 1989.

[20] S. Rao, D. Wilton, and A. Glisson, "Electromagnetic scattering by surfaces of arbitrary shape," *IEEE Trans. Antennas Propag.*, vol. 30, pp. 409-418, May 1982.

[21] C. A. Balanis, *Antenna Theory: Analysis and Design.* New York, NY: John Wiley & Sons, 1982.

[22] C. G. Montgomery, R. H. Dicke, and E. M. Purcell, *Principles of Microwave Circuits.* New York: McGraw-Hill, 1948.

[23] R. E. Collin, *Foundations for Microwave Engineering.* New York: Wiley-IEEE Press, 2000.

[24] S. Silver, *Microwave Antenna Theory and Design.* New York: McGraw-Hill, 1949.

[25] D. M. Kerns, *Plane-Wave Scattering-Matrix Theory of Antennas and Antenna-Antenna Interactions. Nat. Bur. of Stand. Monog. 162.* Boulder: National Bureau of Standards, 1981.

[26] J. Kennedy, R. C. Eberhart, and Y. Shi, *Swarm Intelligence.* San Francisco: Morgan Kaufmann Publishiers, 2001.

[27] F. van den Bergh, "An analysis of particle swarm optimizers," Ph. D. dissertation, Dept. Comput. Sci., Univ. Pretoria, Pretoria, South Africa, 2002.

[28] S. H. Lee, J. K. Park, and J. N. Lee, "A novel CPW-fed ultra-wideband antenna design," *Microw. Opt. Technol. Lett.*, vol. 44, no. 5, pp. 393-396, Mar. 2005.

Figure Captions

- **Figure 1.** Descriptive parameters of the spline-based antenna representation.

- **Figure 2.** Schematic representation of (a) the system constituted by a couple of identical antennas, (b) the antenna and reflecting surface configuration, (c) the equivalent image configuration, and (d) the single antenna radiating in free-space.

- **Figure 3.** *Test Case 1* ($f^{(min)} = 6\,GHz$, $f^{(max)} = 9\,GHz$, ECC standard, $N = 4$) - Evolution of the antenna shape: (a) $k = 0$, (b) $k = 10$, (c) $k = 19$, and (d) $k = k_{conv} = 28$.

- **Figure 4.** *Test Case 1* ($f^{(min)} = 6\,GHz$, $f^{(max)} = 9\,GHz$, ECC standard, $N = 4$) - Plot of (a) $\left|s_{11}\left\{AGG\left(\underline{\varsigma}^{(k)}\right)\right\}\right|$, (b) $\left|s_{21}\left\{AGG\left(\underline{\varsigma}^{(k)}\right)\right\}\right|$, (c) $\angle s_{21}\left\{AGG\left(\underline{\varsigma}^{(k)}\right)\right\}$, and (d) $\tau\left\{AGG\left(\underline{\varsigma}^{(k)}\right)\right\}$ versus the frequency at different iterations of the optimization process.

- **Figure 5.** *Test Case 1 - Parametric approach* - Descriptive parameters for the circular monopole reference geometry.

- **Figure 6.** *Test Case 1 - Parametric Approach* ($f^{(min)} = 6\,GHz$, $f^{(max)} = 9\,GHz$, ECC standard) - Evolution of the antenna shape: (a) $k = 0$, (b) $k = 100$, (c) $k = 300$, and (d) $k = K = 400$.

- **Figure 7.** *Test Case 1 - Parametric Approach* ($f^{(min)} = 6\,GHz$, $f^{(max)} = 9\,GHz$, ECC standard) - Plot of (a) $\left|s_{11}\left\{AGG\left(\underline{\varsigma}^{(k)}\right)\right\}\right|$, (b) $\left|s_{21}\left\{AGG\left(\underline{\varsigma}^{(k)}\right)\right\}\right|$, (c) $\angle s_{21}\left\{AGG\left(\underline{\varsigma}^{(k)}\right)\right\}$, and (d) $\tau\left\{AGG\left(\underline{\varsigma}^{(k)}\right)\right\}$ versus the frequency at different iterations of the optimization process.

- **Figure 8.** *Test Case 1* ($f^{(min)} = 6\,GHz$, $f^{(max)} = 9\,GHz$, ECC standard, $N = 4$) - Comparison between parametric approach and spline-based approach - Plot of the optimal value of the cost function $\Omega\left[AGG\left(\underline{\varsigma}^{(k)}\right)\right]$ and corresponding terms versus the iteration number k.

- **Figure 9.** *Test Case 1* ($f^{(min)} = 6\,GHz$, $f^{(max)} = 9\,GHz$, ECC standard) - Behavior of the quality indexes F_{11}, F_{21}, F_{GD} and of k_{conv} versus the number of control

points N.

- **Figure 10.** *Test Case 2* ($f^{(min)} = 4\,GHz$, $f^{(max)} = 9\,GHz$, FCC standard, $N = 7$) - Antenna prototype: (a) front view and (b) back view.

- **Figure 11.** *Test Case 2* ($f^{(min)} = 4\,GHz$, $f^{(max)} = 9\,GHz$, FCC standard, $N = 7$) - Numerical and measured values of (a) $|\widehat{s}_{11}|$, (b) $|\widehat{s}_{21}|$, (c) $\angle\widehat{s}_{21}$, and (d) $\widehat{\tau}$ versus the frequency f.

- **Figure 12.** *Test Case 3* ($f^{(min)} = 4\,GHz$, $f^{(max)} = 10\,GHz$, $\varphi_1^{(max)} = 35\,mm$, $\varphi_2^{(max)} = 15\,mm$, FCC standard, $N = 7$) - Numerical and measured values of (a) $|\widehat{s}_{11}|$, (b) $|\widehat{s}_{21}|$, (c) $\angle\widehat{s}_{21}$, and (d) $\widehat{\tau}$ versus the frequency f.

- **Figure 13.** *Test Case 3* ($f^{(min)} = 4\,GHz$, $f^{(max)} = 10\,GHz$, $\varphi_1^{(max)} = 35\,mm$, $\varphi_2^{(max)} = 15\,mm$, FCC standard, $N = 7$) - Antenna prototype: (a) front view and (b) back view.

Table Captions

- **Table I.** *Test Case 2* ($f^{(min)} = 4\,GHz$, $f^{(max)} = 9\,GHz$, FCC standard, $N = 7$) - Geometric descriptors and electric parameters of the synthesized antenna.

- **Table II.** *Test Case 3* ($f^{(min)} = 4\,GHz$, $f^{(max)} = 10\,GHz$, $\varphi_1^{(max)} = 35\,mm$, $\varphi_2^{(max)} = 15\,mm$, FCC standard, $N = 7$) - Geometric descriptors and electric parameters of the synthesized antenna.

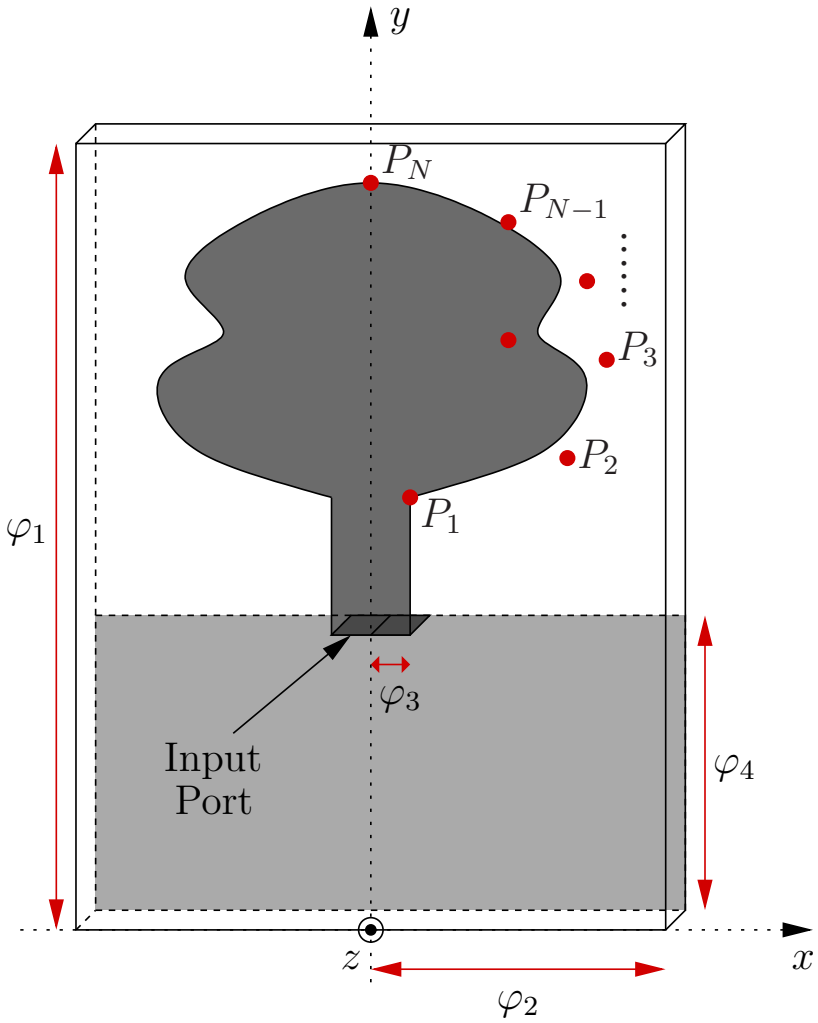

Fig. 1 - L. Lizzi *et al.*, "A Spline-based Shaping Approach for Ultra-Wideband ..."

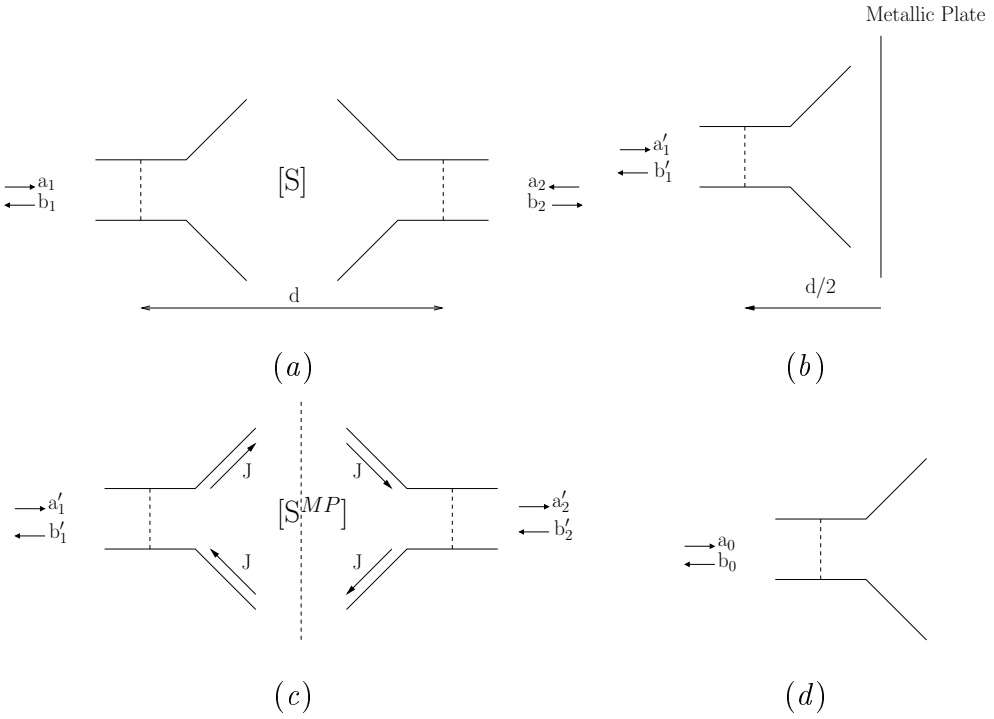

Fig. 2 - L. Lizzi *et al.*, "A Spline-based Shaping Approach for Ultra-Wideband ..."

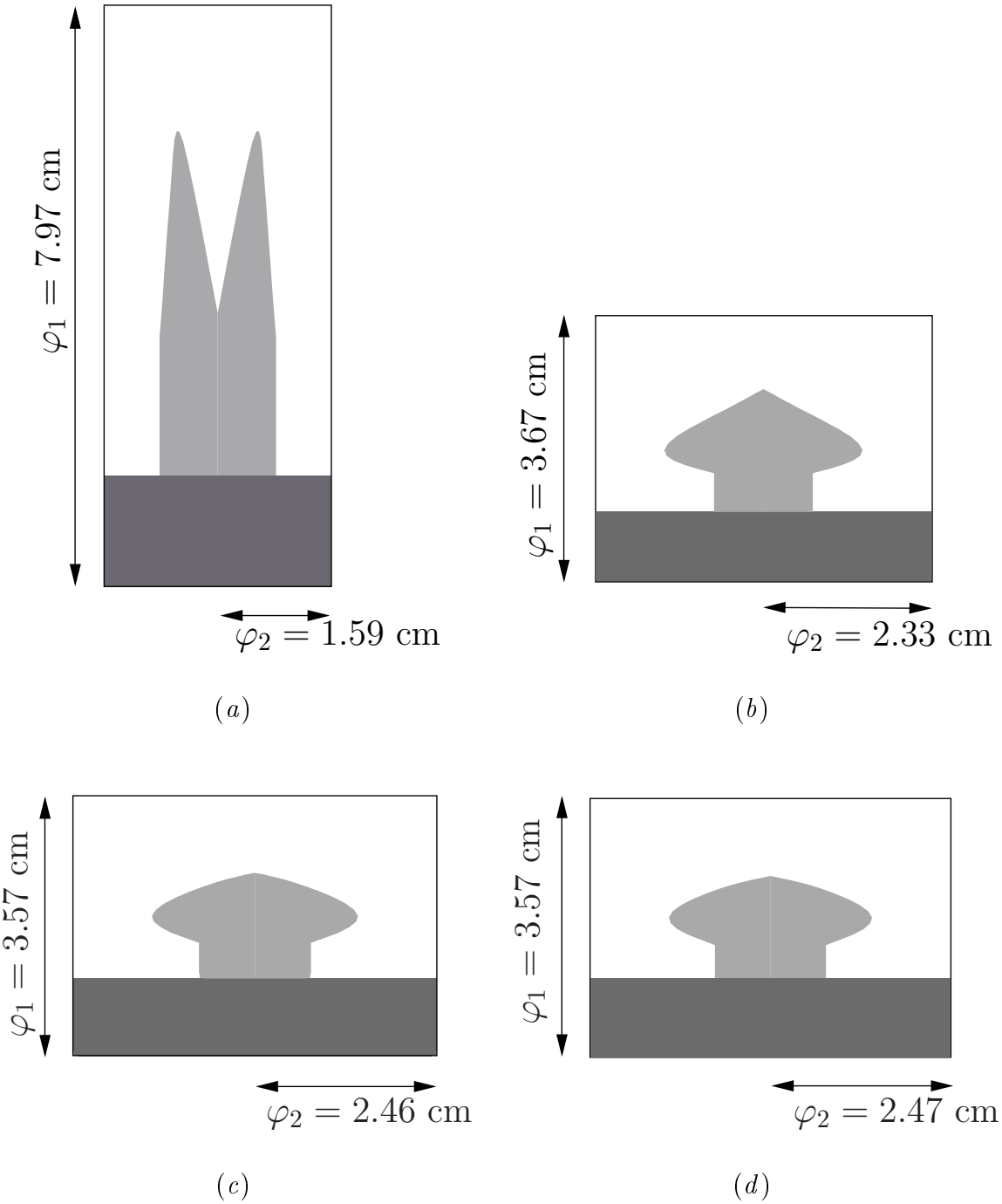

Fig. 3 - L. Lizzi *et al.*, "A Spline-based Shaping Approach for Ultra-Wideband ..."

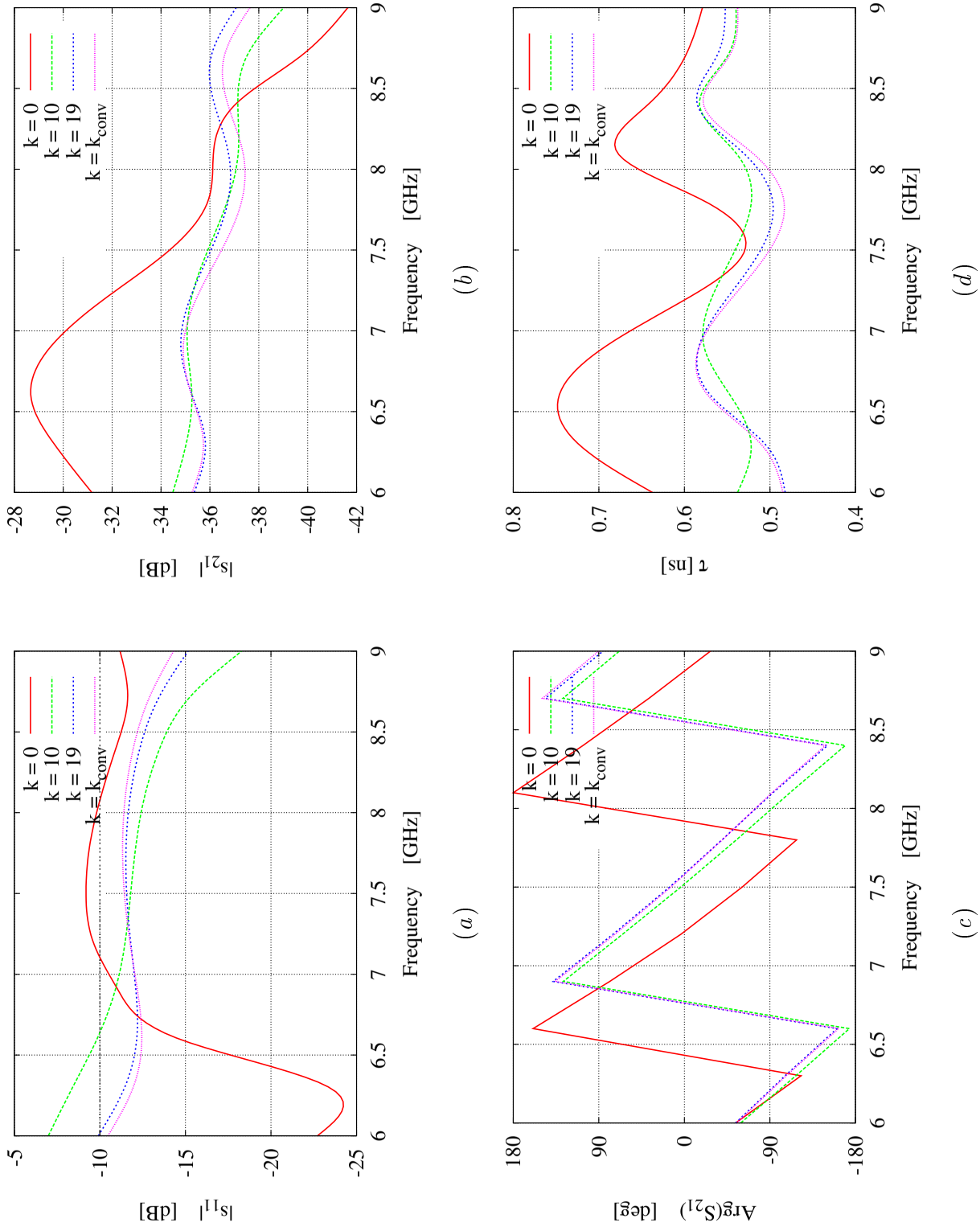

Fig. 4 - L. Lizzi *et al.*, "A Spline-based Shaping Approach for Ultra-Wideband ..."

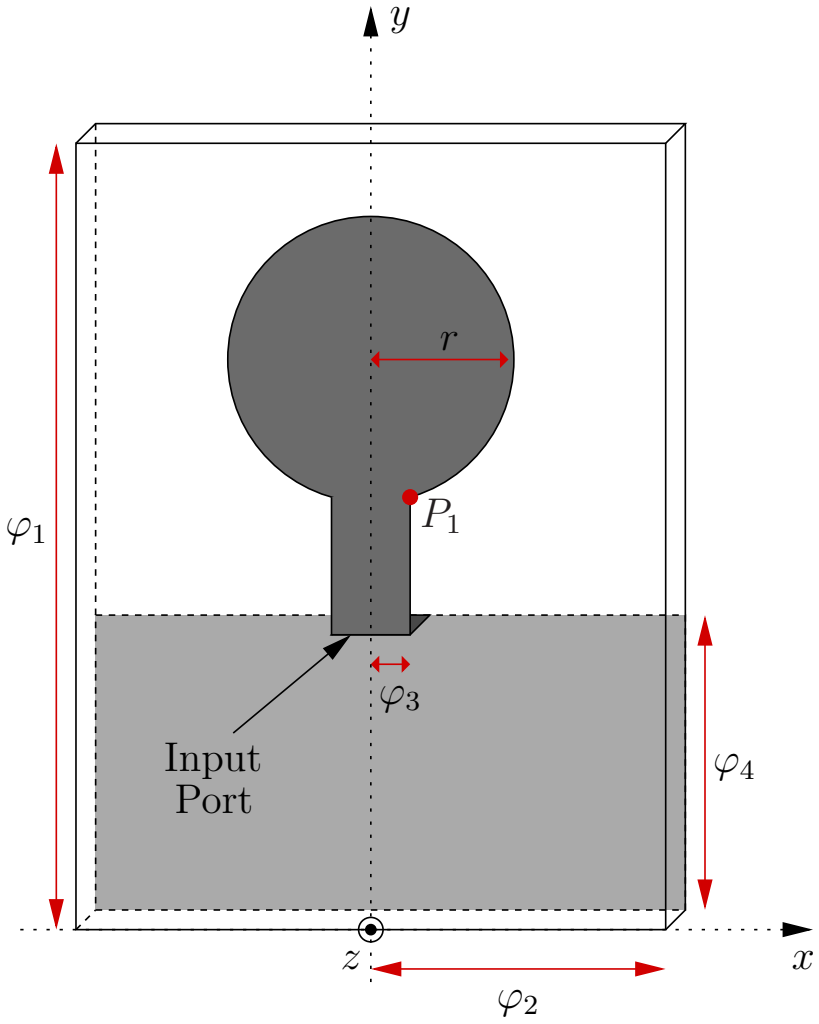

Fig. 5 - L. Lizzi *et al.*, "A Spline-based Shaping Approach for Ultra-Wideband ..."

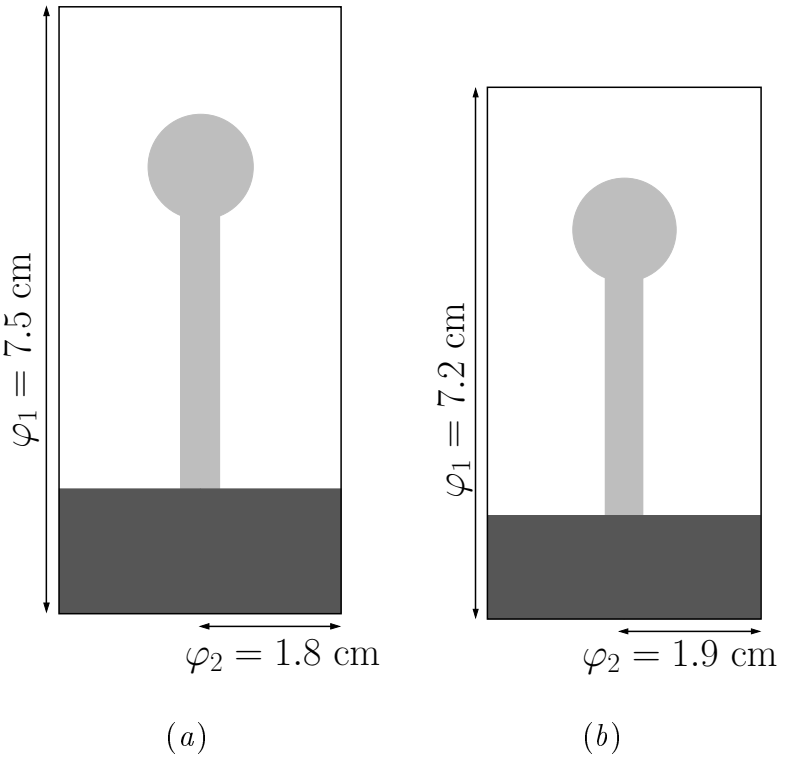

Fig. 6 - L. Lizzi *et al.*, "A Spline-based Shaping Approach for Ultra-Wideband ..."

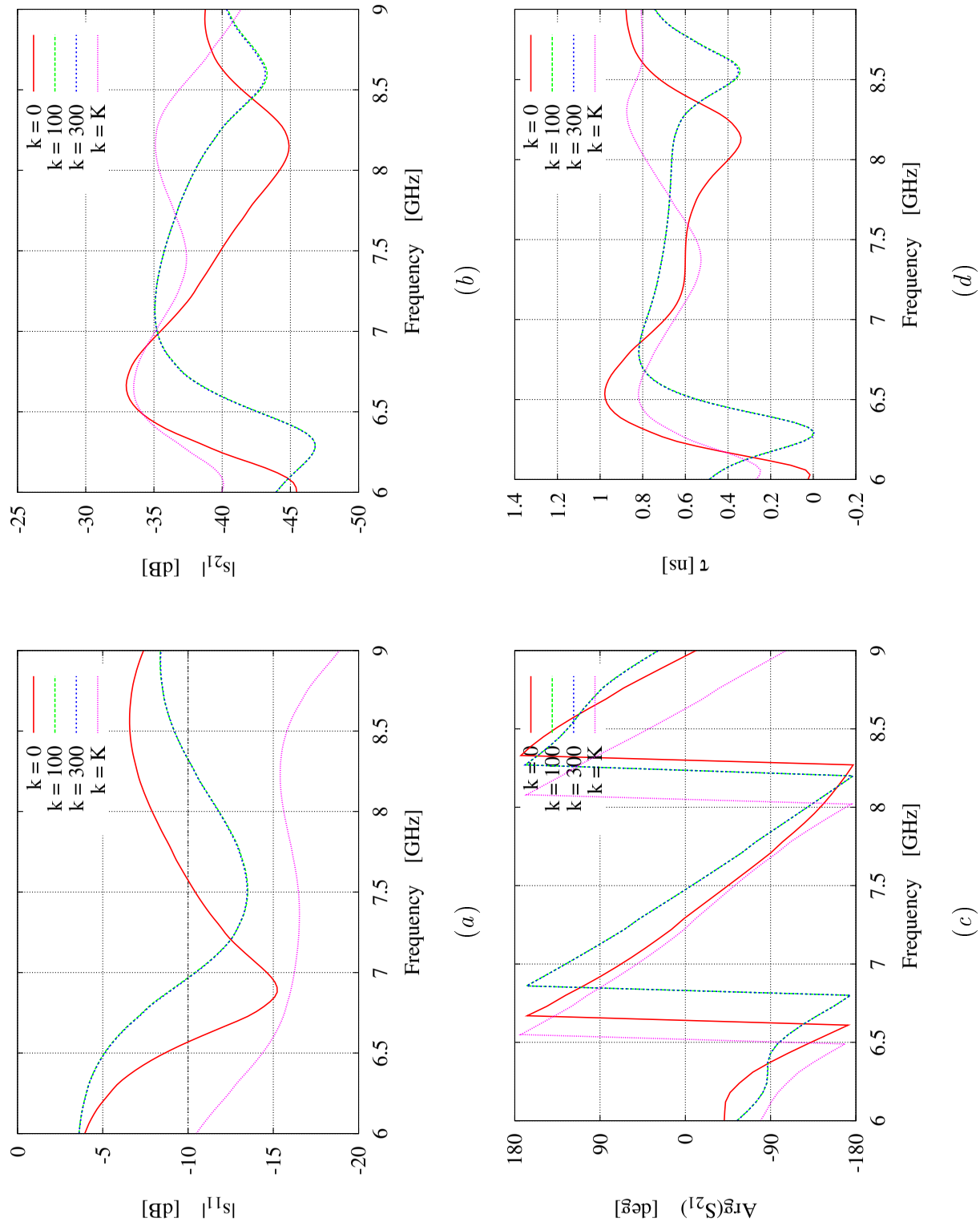

Fig. 7 - L. Lizzi *et al.*, "A Spline-based Shaping Approach for Ultra-Wideband ..."

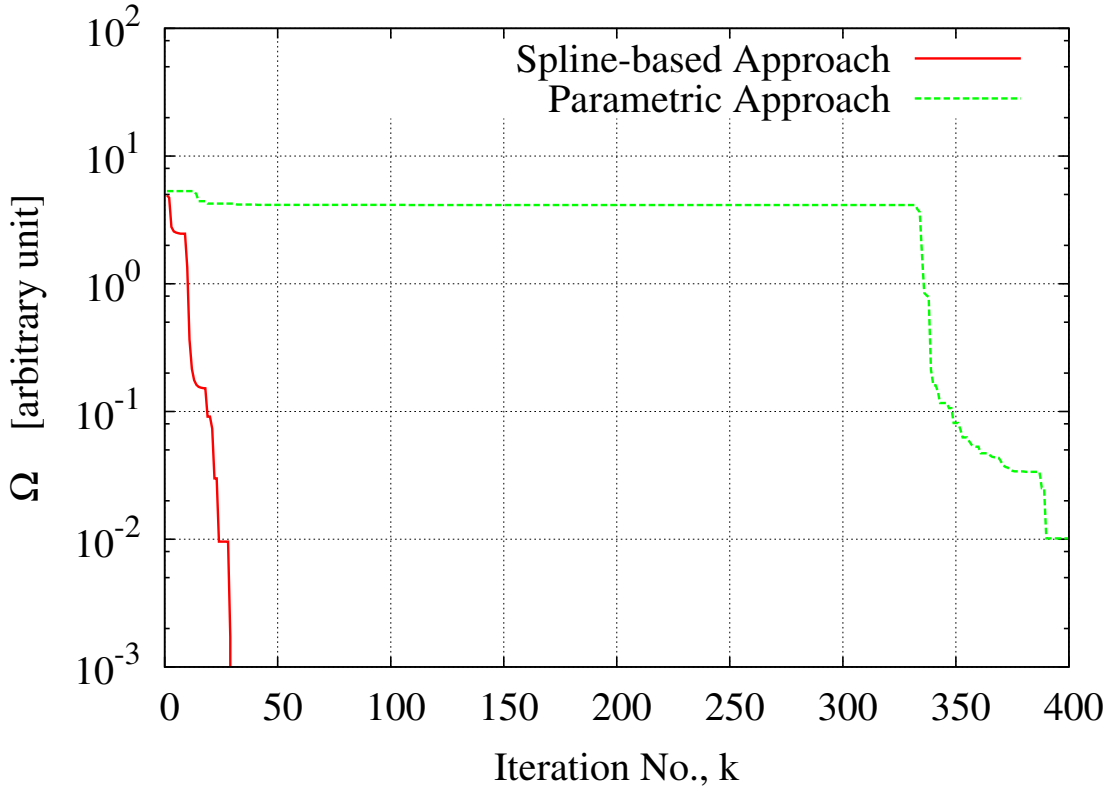

Fig. 8 - L. Lizzi *et al.*, "A Spline-based Shaping Approach for Ultra-Wideband ..."

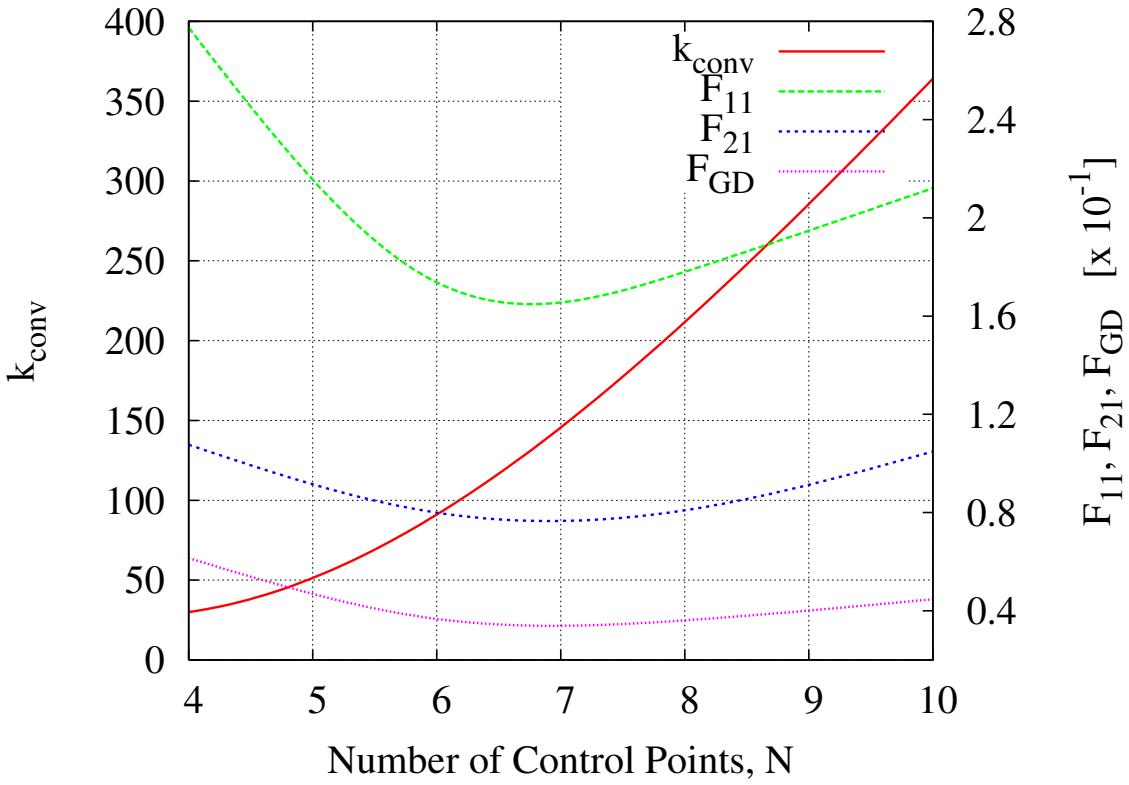

Fig. 9 - L. Lizzi *et al.*, "A Spline-based Shaping Approach for Ultra-Wideband ..."

(a)

(b)

Fig. 10 - L. Lizzi *et al.*, "A Spline-based Shaping Approach for Ultra-Wideband ..."

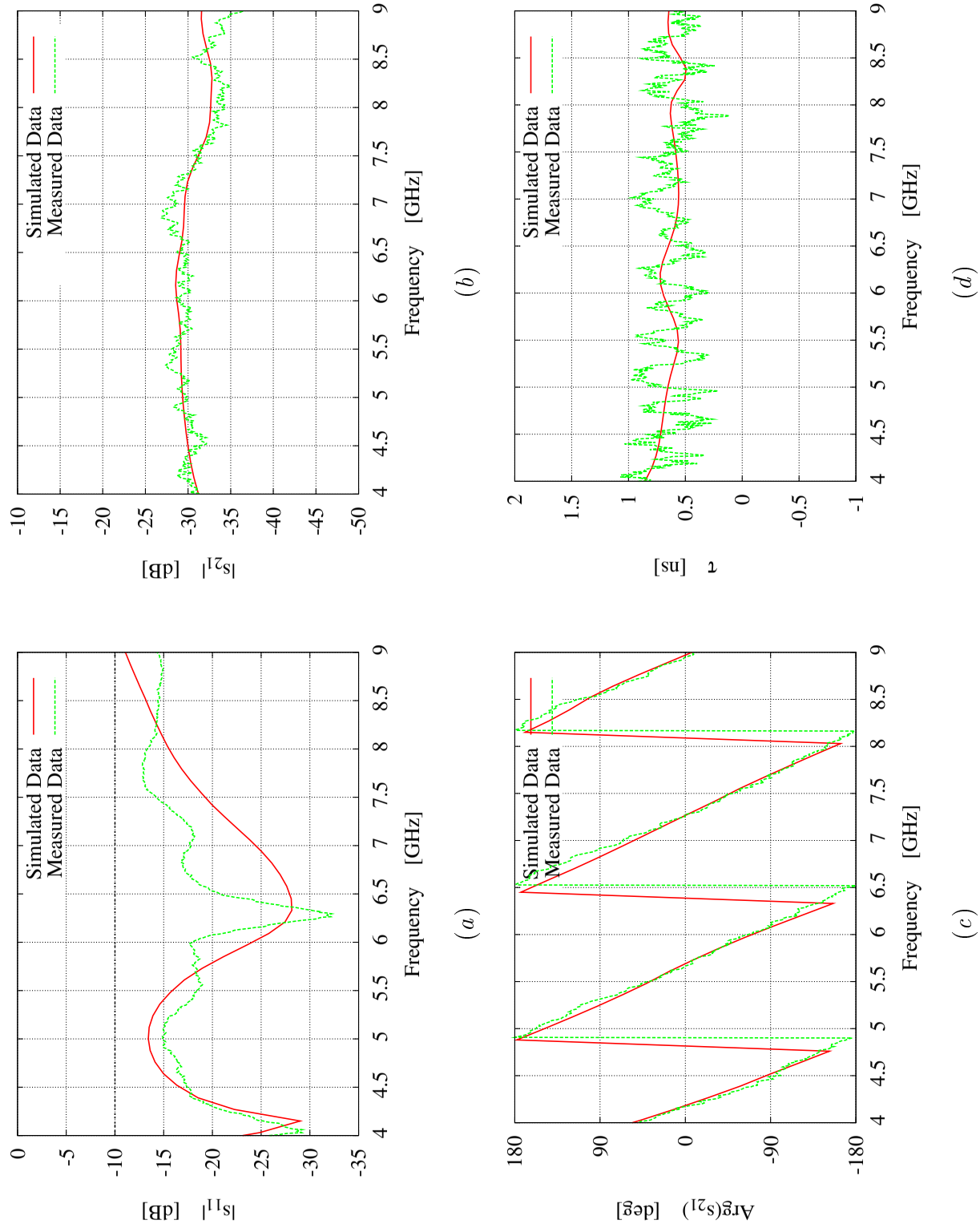

Fig. 11 - L. Lizzi *et al.*, "A Spline-based Shaping Approach for Ultra-Wideband ..."

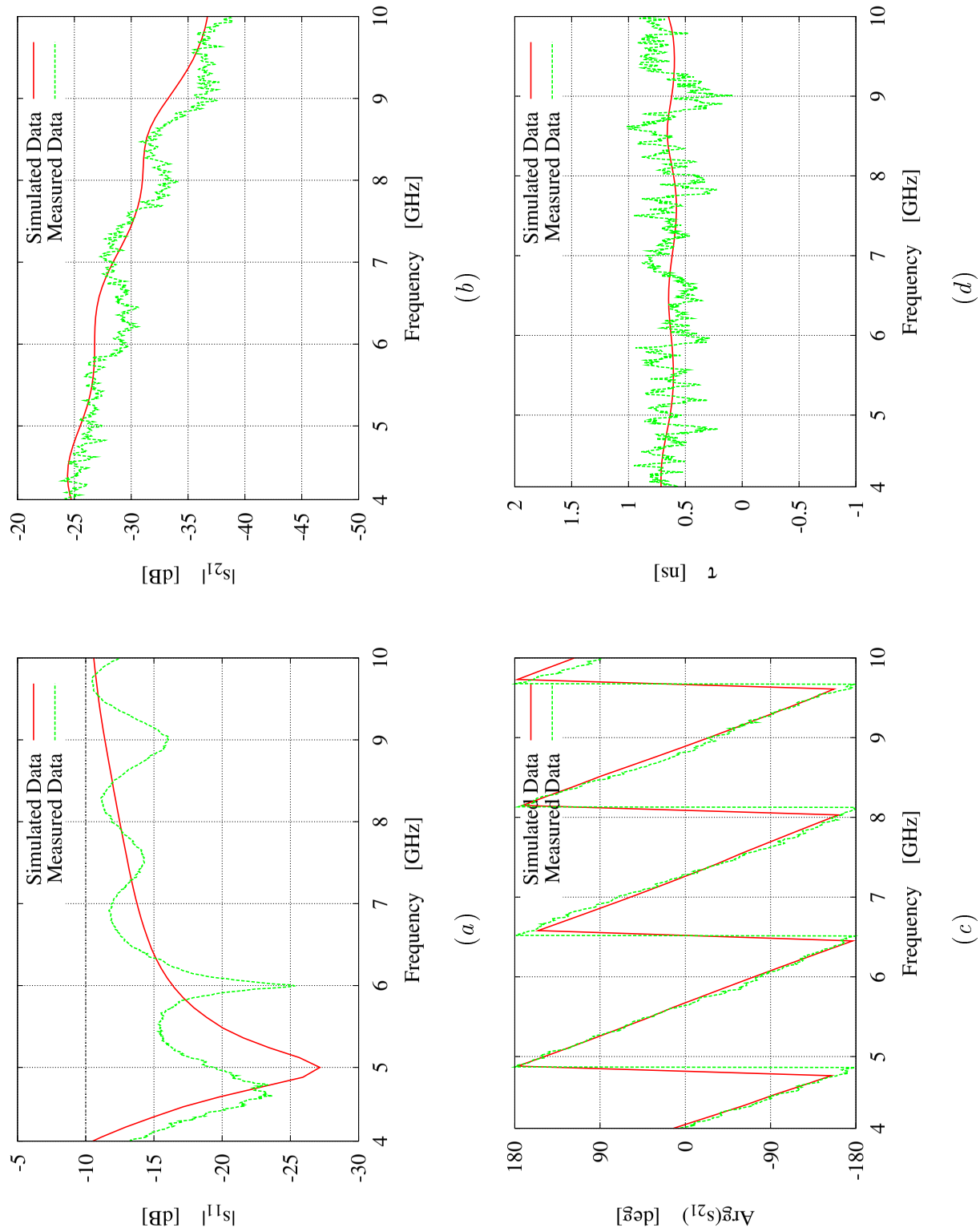

Fig. 12 - L. Lizzi *et al.*, "A Spline-based Shaping Approach for Ultra-Wideband ..."

(a)

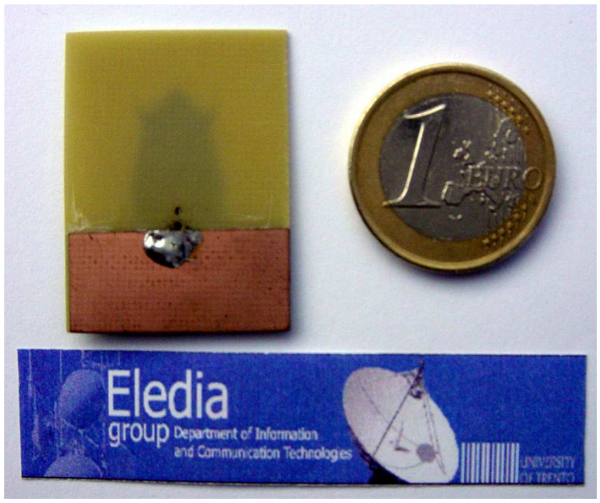

(b)

Fig. 13 - L. Lizzi *et al.*, "A Spline-based Shaping Approach for Ultra-Wideband ..."

Test Case 2							
Control Points Coordinates [mm]							
x_1	y_1	x_2	y_2	x_3	y_3	x_4	y_4
5.4	51.6	6.9	57.6	9.0	60.6	7.0	65.1
x_5		y_5	x_6	y_6	x_7	y_7	
2.7		67.3	2.0	64.5	0.0	56.0	
Geometric Variables [mm]							
φ_1		φ_2		φ_3		φ_4	
69.2		10.0		5.4		10.9	
Performance							
$\triangle f \quad [GHz]$		$\triangle \lvert s_{21} \rvert \quad [dB]$				$\triangle \tau \quad [ns]$	
5 (4-9)		5				0.5	

Tab. I - L. Lizzi *et al.*, "A Spline-based Shaping Approach for Ultra-Wideband ..."

Test Case 3							
Control Points Coordinates [mm]							
x_1	y_1	x_2	y_2	x_3	y_3	x_4	y_4
5.0	14.7	5.2	17.1	3.1	22.5	5.1	25.7
x_5		y_5	x_6	y_6	x_7	y_7	
3.3		24.7	3.8	23.0	0.0	27.2	
Geometric Variables [mm]							
φ_1		φ_2		φ_3		φ_4	
33.3		12.2		5.0		12.2	
Performance							
$\triangle f \quad [GHz]$		$\triangle \lvert S_{21} \rvert \quad [dB]$				$\triangle \tau \quad [ns]$	
6 (4-10)		12				0.15	

Tab. II - L. Lizzi *et al.*, "A Spline-based Shaping Approach for Ultra-Wideband ..."